Inorganic Chemistry

pubs.acs.org/IC Article

Chromium(0) and Molydenum(0) Complexes with a Pyridyl-Mesoionic Carbene Ligand: Structural, (Spectro)electrochemical, Photochemical, and Theoretical Investigations

Tobias Bens, Pit Boden, Patrick Di Martino-Fumo, Julia Beerhues, Uta Albold, Sebastian Sobottka, Nicolás I. Neuman, Markus Gerhards,* and Biprajit Sarkar*

Cite This: https://dx.doi.org/10.1021/acs.inorgchem.0c02537 Read Online

ACCESS | Metrics & More | Article Recommendations | Supporting Information

ABSTRACT: This work reports on the synthesis and in-depth electrochemical and photochemical characterization of two chromium(0) and molydenum(0) metal complexes with bidentate pyridyl-mesoionic carbene (MIC) ligands of the 1,2,3-triazol-5-ylidene type and carbonyl coligands. Metal complexes with MIC ligands have turned out to have very promising electrocatalytic and photochemical properties, but examples of MIC-containing complexes with early-transition-metal centers remain extremely rare. The electrochemistry of these new MIC complexes was studied by cyclic voltammetry and especially spectroelectrochemistry in the IR region consistent with a mainly metal-centered oxidation, which is fully reversible in the case of the chromium(0) complex. At the same time, the two reduction steps are predominantly ligand-centered according to the observed near-IR absorbance, with the first reduction step being reversible for both systems. The results of the electron paramagnetic resonance studies on the oxidized and reduced species confirm the IR spectroelectrochemistry experiments. The photochemical reactivity of the complexes with a series of organic ligands was investigated by time-resolved (step-scan) Fourier transform infrared (FTIR) spectroscopy. Interestingly, the photoreactions in pyridine and acetonitrile are fully reversible with a slow dark reverse reaction back to the educt species over minutes and even hours, depending on the metal center and reagent. This reversible behavior is in contrast to the expected loss of one or several CO ligands known from related homoleptic as well as heteroleptic $M(CO)_4L_2$ α-diimine transition-metal complexes.

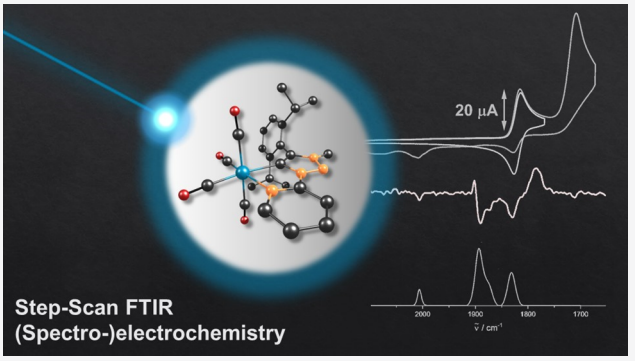

INTRODUCTION

Mesoionic carbenes (MICs) of the 1,2,3-triazol-5-ylidene type have established themselves as prominent ligands in organometallic chemistry.[1−6] While in the majority of cases these ligands have been used in homogeneous catalysis,[3−6] they have also found applications in small-molecule activation[7−11] and as parts of redox-active metal complexes.[12,13] Furthermore, such ligands have also been used in the field of photochemistry[14−23] and in redox-induced and redox-switchable catalysis.[24−28] Metal complexes of bidentate ligands containing one MIC and one pyridyl donor have displayed excellent photochemical[9,19,23] and electrocatalytic properties.[10] Most of the aforementioned metal complexes are predominantly based on late transition metals.[3−6] Examples of early transition metals with MIC ligands remain extremely rare.[29] As part of our continued interest in the transition-metal chemistry of bidentate pyridyl-MIC-type ligands, we have now turned our attention to the group 6 metals chromium and molybdenum. The carbonyl coligands on the Cr^0 and Mo^0 centers make them ideal platforms for a number of electrochemical and spectroscopic (including photochemical and photophysical) investigations.[30−33] In particular, the CO ligands are powerful markers for IR spectroscopy and can be very conveniently used for following excited-state dynamics and reactivity in these metal complexes. In this context, time-resolved step-scan Fourier transform infrared (FTIR) spectroscopy turned out to be an ideal tool to characterize the long-lived electronically excited states of transition-metal complexes on time scales of nanoseconds and microseconds.[34−39] At the same time, the step-scan technique has been successfully applied in the analysis of the photoinduced reactions[35,40,41] also involving transition metals.[42−44]

In the following, we present the synthesis and characterization of the chromium(0) and molydenum(0) complexes **1**

Received: August 25, 2020

https://dx.doi.org/10.1021/acs.inorgchem.0c02537
Inorg. Chem. XXXX, XXX, XXX−XXX

and **2** that contain the bidentate MIC-containing ligand **L** and additional CO coligands. The electronic structures were investigated by UV−vis−near-IR (NIR), IR, and electron paramagnetic resonance (EPR) spectroelectrochemical measurements for both complexes, in combination with density functional theory (DFT) calculations. Furthermore, the photochemical reactivity was studied by time-resolved FTIR spectroscopy to probe the dynamics and ligand-exchange reactions of these complexes in the excited state. The choice of ligand **L** for these investigations is interesting because **L** has certain similarities to the α-diimine ligands mentioned above. However, **L** possesses two different donors, and one of them is the strongly donating MIC, which is expected to have a profound influence on the properties of the resulting metal complexes. To the best of our knowledge, these are the first thorough investigations of transition-metal-bound radicals that are based on MIC ligands of the 1,2,3-triazol-5-ylidene type.

Additionally, these are also the first spectroscopic investigations using time-resolved FTIR spectroscopy on the light-induced ligand substitution reactions in transition-metal complexes containing MIC ligands.

RESULTS AND DISCUSSION

Synthesis and Characterization. The pyridyltriazolium salt [**HL1**]OTf was synthesized by using a five-step synthetic route in reasonable yield (see Scheme 1 and the Supporting Information). Despite the presence of an additional pyridyl N atom in **E6**, methylation of this compound with MeOTf was fairly selective.

Scheme 1. Synthetic Strategy for [HL1]OTf

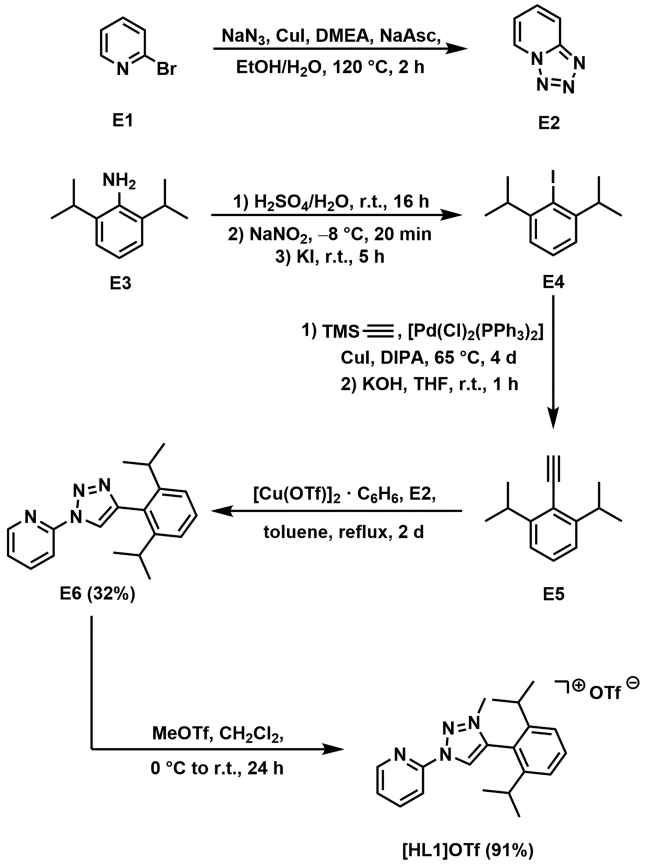

For the synthesis of complex **1**, $Cr(CO)_6$ was irradiated with UV light in tetrahydrofuran (THF; Scheme 2). The in situ formed solvato complex was further reacted with [**HL1**]OTf in the presence of NEt_3 as a base. Extractions and further chromatographic purification delivered complex **1** in good yield. A similar strategy was also used for the synthesis of complex **2**, except that in this case the prior formation of the norbornadiene complex from $Mo(CO)_6$ was necessary to get better product yield (Scheme 2). The identity and purity of the complexes were ascertained by NMR spectroscopy, elemental analysis, and electrospray ionization mass spectrometry.

We were able to obtain suitable single crystals for performing single-crystal X-ray diffraction studies. A look at the molecular structure in the crystal for both complexes (Figure 1) shows that the metal centers are coordinated in a distorted octahedral environment, with the distortion being imposed by the chelating nature of the **L1** ligand.

The Cr−C and Cr−N bond lengths to the MIC and pyridyl donors of **L1** are 2.065(2) and 2.147(2) Å. The corresponding Mo−C and Mo−N bond lengths in **2** are 2.202(1) and 2.275(1) Å. These differences in the bond lengths are a result of the different sizes of the two metal centers. The M−C bond lengths to the CO ligands that are trans to each other are longer than the M−C bond lengths to the CO ligands that are trans to **L1**. Accordingly, the C−O bond distances within the CO ligands that are trans to each other are shorter compared the same distances within the CO ligands that are trans to **L1** (Table S1). Both of these effects are likely related to the better trans influence of **L1** compared to that of the CO ligands. The C−C and C−N bond lengths within the **L1** ligand in both complexes **1** and **2** are all in the expected range.[3−6] The Dipp substituent on the 1,2,3-triazol-5-ylidene ligand in both **1** and **2** is twisted out-of-plane, with the dihedral angles between the two planes being 79.1(1)° and 79.5(1)°.

Electrochemistry and Spectroelectrochemistry. Both complexes **1** and **2** display oxidation steps at −0.17 and +0.08 V (Figure 2; all measurements were carried out in CH_3CN/0.1 M Bu_4NPF_6 and referenced against the FcH/FcH^+ couple).

These data show that both of these complexes are easy to oxidize, a fact that is a reflection of the low oxidation state of the metal centers combined with the strongly donating nature of the MIC-containing ligand.

The oxidation step for the chromium complex **1** is reversible, whereas that for the molybdenum complex **2** is irreversible. As reported previously,[45,46] we attribute this behavior to a more facile labilization of the M−CO bond upon oxidation for the molybdenum complex compared to the chromium complex. Notably, with the ligand **L1**, the oxidation step in complex **1** is reversible at ambient temperatures at normal scan rates (100 mV/s). For related α-diimine-containing $[Cr(CO)_4]$ complexes, usually lower temperatures, higher scan rates, or both are necessary to obtain reversibility.[47] We attribute the higher reversibility in our case to the presence of the strongly donating MIC unit in **L1**, which is likely able to compensate for the electron loss at the Cr center that is induced through oxidation.

Both complexes also display two reduction steps each (Figure 3). The first reduction steps, which are observed for **1** and **2** at −2.16 and −2.10 V, are reversible. The second reduction steps for these complexes appear at −2.79 and −2.68 V. This step is electrochemically and chemically irreversible for both complexes (Figure 3) because the second

https://dx.doi.org/10.1021/acs.inorgchem.0c02537
Inorg. Chem. XXXX, XXX, XXX−XXX

Scheme 2. Synthetic Strategy for 1 and 2

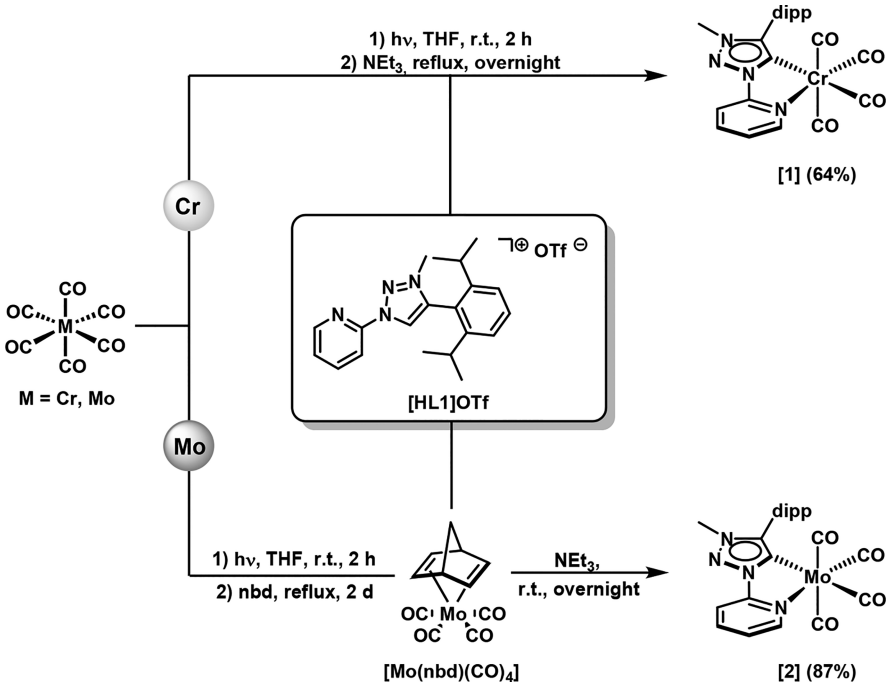

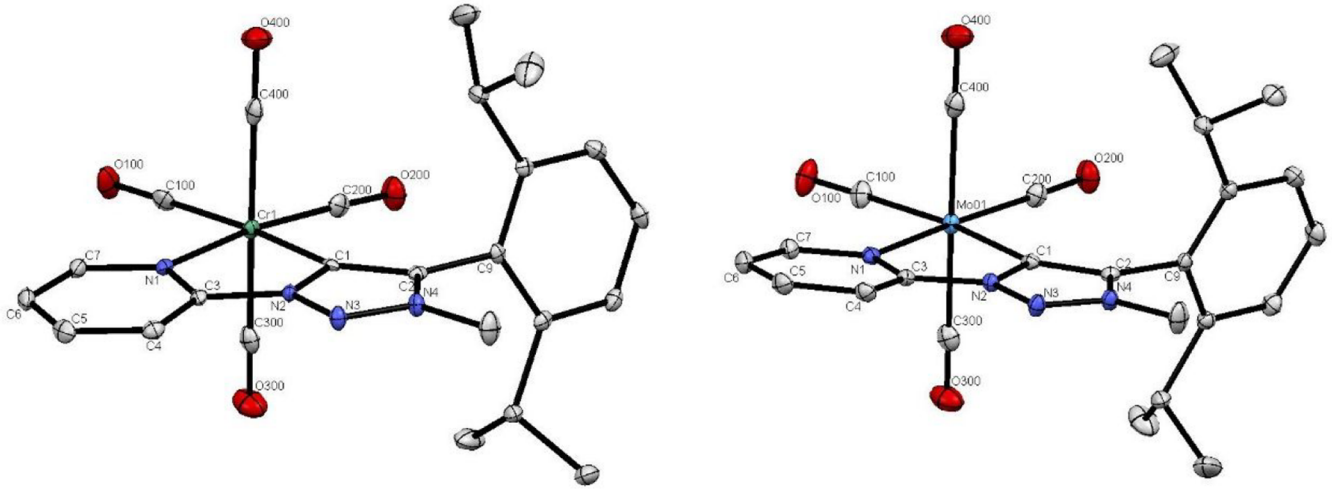

Figure 1. ORTEP representations of **1** (left) and **2** (right). H atoms are omitted for clarity. Ellipsoids are drawn with 50% probability.

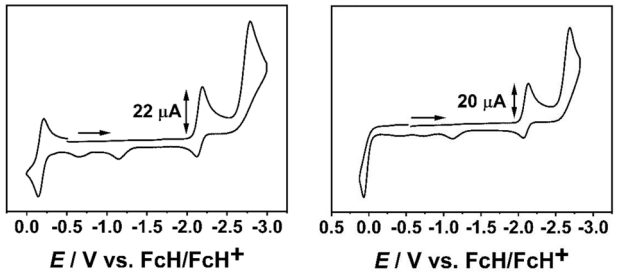

Figure 2. Cyclic voltammograms of **1** (left) and **2** (right) in CH_3CN/0.1 M Bu_4NPF_6 with a glassy carbon working electrode at a scan rate of 100 mV/s.

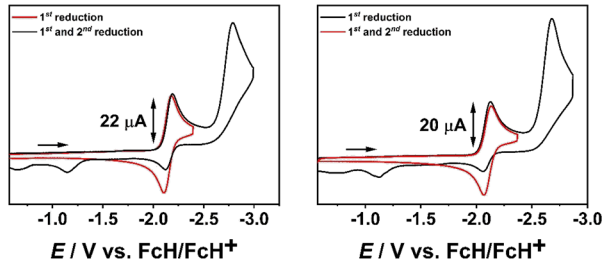

Figure 3. Cyclic voltammograms of **1** (left) and **2** (right) in CH_3CN/0.1 M Bu_4NPF_6 with a glassy carbon working electrode at a scan rate of 100 mV/s (red, first reduction; black, first and second reduction).

reduction step leads to the appearance of at least two reoxidation peaks that are shifted far to the positive side, indicating the irreversible nature of that reduction step.

As can be seen from above, the oxidation potentials for the two complexes differ substantially from each other, whereas the reduction potentials are fairly similar. These data are a first indication of a predominantly metal-centered oxidation and a

https://dx.doi.org/10.1021/acs.inorgchem.0c02537
Inorg. Chem. XXXX, XXX, XXX−XXX

predominantly ligand-centered reduction. A more direct proof of these assignments comes from spectroelectrochemical studies and DFT calculations as discussed below.

The IR spectra of **1** and **2** in CH_3CN both display a four-band pattern in the region of 1830−2010 cm^{-1} typical for the stretching vibrations of CO ligands (Figures 4 and S19 and Tables S6 and S8), with the two middle bands being almost degenerate. This pattern is characteristic for group 6 $[M(CO)_4]$ complexes containing an additional bidentate ligand and is similar to what has been observed previously for such complexes with α-diimine ligands.[30−33] The oxidation of **1** to $\mathbf{1}^+$ leads to a strong shift of all of the CO bands to higher energies (Figure 4 and Table S6). For example, the band at 1998 cm^{-1} for **1** is shifted to 2089 cm^{-1} for $\mathbf{1}^+$, which is a change of 91 cm^{-1}. The other bands are also shifted accordingly to higher energies. Additionally, the bands at lower energies become more degenerate for $\mathbf{1}^+$, and the intensities of all the bands are more equal in the oxidized complex compared to the neutral form (Figure 4). The large shift (ca. 90 cm^{-1}) to higher energies of the CO bands is an indication of a metal-centered oxidation step. When the potential was returned to the starting potential after a full oxidation cycle was run, the spectrum of the starting complex was recovered quantitatively, thus displaying the reversibility of the oxidation step in **1**, also on the IR spectroelectrochemistry time scale (Figure S14). Even though the oxidation step of complex **2** is not reversible, the spectral shifts and intensities and the pattern observed in the IR spectrum of the oxidized species as well as a comparison of the spectrum with that of $\mathbf{1}^+$ indicate a metal-centered oxidation also for **2** (Figure S18 and Table S8).

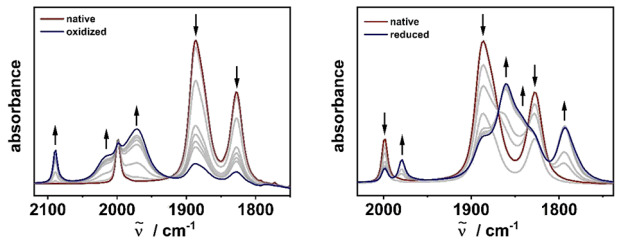

Figure 4. Changes in the IR spectra of **1** in CH_3CN/0.1 M Bu_4NPF_6 with a gold working electrode during the first oxidation (left) and first reduction (right).

In contrast to the oxidation step, the first reduction leads to a shift of all the CO bands to lower energies (Figures 4 and S19 and Tables S6 and S8). The extent of the band shifts is much smaller for the reduction step compared to the oxidation step. For example, the high energy band at 1998 cm^{-1} in **1** is only shifted to 1978 cm^{-1} in $\mathbf{1}^{\bullet-}$, which is just a difference of 20 cm^{-1}. A similar pattern is also observed for the conversion of **2** to $\mathbf{2}^{\bullet-}$. The small shift of the CO bands upon one-electron reduction is an indication of a predominantly **L1**-centered reduction step (see below). For both complexes **1** and **2**, running a complete first reduction and reoxidation back to the starting potential led to an almost quantitative regeneration of the starting spectrum, thus displaying the reversible nature of the first reduction step for both complexes (Figures S15 and S19).

The in situ generated one-electron-oxidized species $\mathbf{1}^+$ did not display any EPR signal in a fluid solution at ambient temperatures. In a frozen solution at −130 °C, $\mathbf{1}^+$ displays a signal with axial anisotropy with $g_{\parallel}$ = 1.980 and $g_{\perp}$ = 2.062, with Δ = 0.082. The simulated spectrum, including hyperfine coupling to the ^{53}Cr nucleus ($I = {}^3/_2$; natural abundance = 9.5%), fits nicely with the experimental spectrum (Figure 5). The absence of a signal in a fluid solution at room temperature and the substantial g anisotropy observed in a frozen solution indicate a predominantly metal-centered spin.

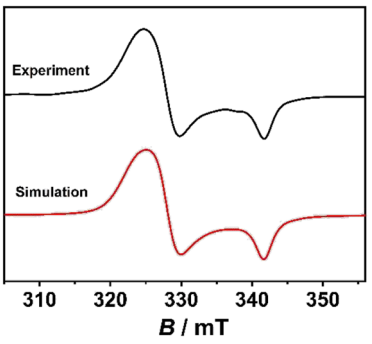

Figure 5. EPR spectrum of in situ generated $\mathbf{1}^+$ at −130 °C in CH_3CN/0.1 M Bu_4NPF_6.

The in situ generated reduced forms $\mathbf{1}^{\bullet-}$ and $\mathbf{2}^{\bullet-}$ display line-rich spectra in a fluid solution at ambient temperatures, centered at g = 2.003 and 2.004 (Figure 6). Both spectra could be simulated with good accuracy by considering a very small hyperfine coupling to the respective metal centers and predominant hyperfine couplings to four different ^{14}N nuclei and three or four different ^1H nuclei. These results suggest that the spin in the reduced complexes is predominantly localized on the MIC and pyridyl parts of the **L1** ligand (Tables S29 and S31).

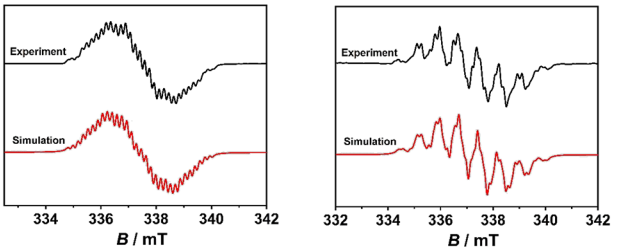

Figure 6. EPR spectra of $\mathbf{1}^{\bullet-}$ (left) and $\mathbf{2}^{\bullet-}$ (right) at room temperature in CH_3CN/0.1 M Bu_4NPF_6.

Spin-density calculations (see below) support these results and also indicate spin densities on only three of the C atoms of the pyridyl rings. The EPR data on the oxidized and reduced complexes thus nicely complement the results from IR spectroelectrochemistry that were discussed above. To the best of our knowledge, this is the first thorough and unambiguous EPR spectroscopic characterization of a metal-bound MIC-containing radical.

Both complexes display two main absorbance bands in the visible region in their native state (Figures 7 and S22 and Tables S10 and S11). These bands have a predominantly metal-to-ligand charge-transfer (MLCT) character [a detailed assignment of the absorption bands observed in the UV−vis−NIR spectra will be made in the (TD-)DFT Calculations section]. The oxidation of complex **1** only leads to a decrease in the intensity of the bands in the visible region, with no other significant changes (Figure S21). In the case of **2**, a new

https://dx.doi.org/10.1021/acs.inorgchem.0c02537
Inorg. Chem. XXXX, XXX, XXX−XXX

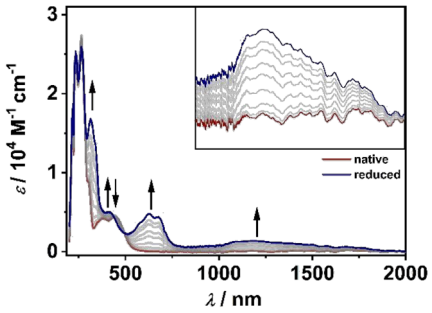

Figure 7. Changes in the UV−vis−NIR spectra of **2** in CH_3CN/0.1 M Bu_4NPF_6 during the first reduction with a gold working electrode (the inset shows the region from 800 to 2000 nm).

absorbance band is observed at about 325 nm upon oxidation, while all of the other bands decrease in intensity (Figure S23). The changes in the visible and NIR regions upon reduction in both complexes are, however, very prominent and interesting.

Both $\mathbf{1}^{\bullet-}$ and $\mathbf{2}^{\bullet-}$ display two low-energy bands in the visible region, as well as a relatively broad band in the NIR region (Figures 7 and S22 and Tables S10 and S11). Such low-energy bands in the visible and NIR regions are often an indication of a metal-bound ligand radical.[48] In view of the results from IR and EPR spectroscopy on the reduced complexes, such an assignment of these long-wavelength bands seems reasonable. A thorough discussion of these assignments will be presented in the (TD-)DFT Calculations section.

Time-Resolved FTIR Spectroscopy. The photochemical reactivity of **1** and **2** with a series of potential organic ligands, namely, CH_3CN, pyridine, 2,2′-bipyridine, and CH_2Cl_2, was analyzed by time-resolved FTIR spectroscopy.

At first, step-scan FTIR investigations were performed on **2** in a CH_3CN solution, where the sample was excited with a 355 nm laser pulse. The negative bleach bands in the step-scan difference spectrum correlate with the educt vibrations and result from a decrease of the educt concentration. The positive bands are assigned to the photoproduct, which is formed upon excitation. The educt vibration at 1831 cm^{-1} is red-shifted to 1785 cm^{-1} in the photoproduct, whereas the initial band at 1894 cm^{-1} is blue-shifted to 1902 cm^{-1}.

The transition observed at 2006 cm^{-1} for the educt is not observed at all upon excitation because only the corresponding bleach without any positive feature is observed (Figure 8).

The pattern and intensities of the step-scan difference spectrum do not change significantly over the entire time range of the experiment (approximately 500 μs after laser excitation), indicating the formation of a long-lived photoproduct (Figure S47). The presented spectra were averaged over 200 μs to obtain smooth spectra with a very good signal-to-noise ratio.

The persistence of the step-scan spectrum over the complete time range of almost 500 μs prompted us to follow the light-induced reaction pathways over longer time scales up to minutes. For this purpose, the sample was irradiated over 5 min at a repetition rate of 100 Hz, which leads to an almost complete disappearance of the educt CO absorption bands. Nevertheless, the remaining weak educt features show that **2** is photochemically quite stable and only reacts under harsh conditions. Interestingly, the new bands observed upon 5 min of irradiation agree perfectly with the positive features seen in the step-scan difference spectrum, so that the same photoproduct is observed independently of the experiment (Figure 9). After the period of irradiation (5 min), the reaction was followed without further UV excitation to analyze potential dark reactions after formation of the mentioned photoproduct. Surprisingly, a slow dark reverse reaction was observed, with complete reformation of the educt after about 30 min and an IR spectrum that is identical with the educt spectrum.

A second period of irradiation (5 min) again leads to the formation of the same changes in the IR spectrum, which underlines the reversibility of the reaction. Hence, the observations definitely do not agree with the mechanism reported for the related homoleptic complex $W(CO)_6$, which was studied by transient IR spectroscopy by Schultz and Krav-Ami.[49] The expected loss of one or several CO ligands, known from homoleptic $M(CO)_6$[50,51] and the related $M(CO)_4L_2$ α-diimine[32,52−54] transition-metal complexes, is not observed here and rather corresponds to cleavage of a coordinative bond of the bidentate MIC ligand to the Mo center and occupation of the free coordination site by a CH_3CN molecule. It is suggested that coordination of the pyridyl moiety of the MIC ligand to the metal center breaks up because the carbene

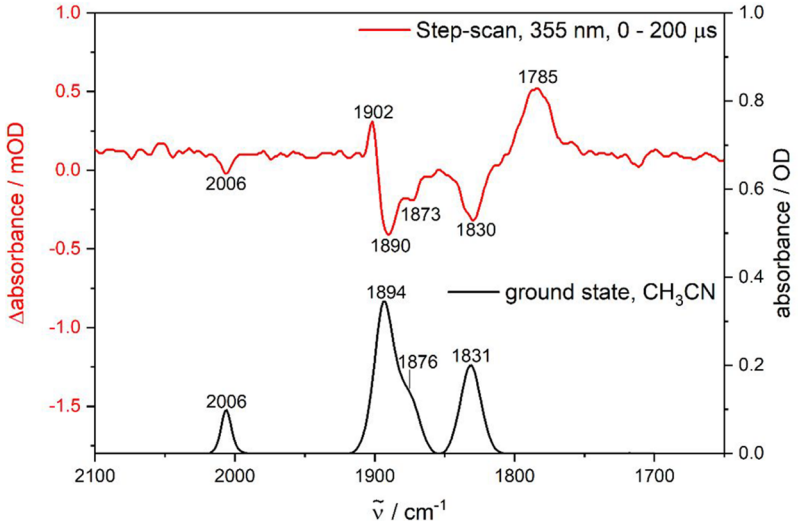

Figure 8. Ground-state FTIR and step-scan difference spectra (λ_{ex} = 355 nm, 0−200 μs) of **2** in CH_3CN.

https://dx.doi.org/10.1021/acs.inorgchem.0c02537
Inorg. Chem. XXXX, XXX, XXX−XXX

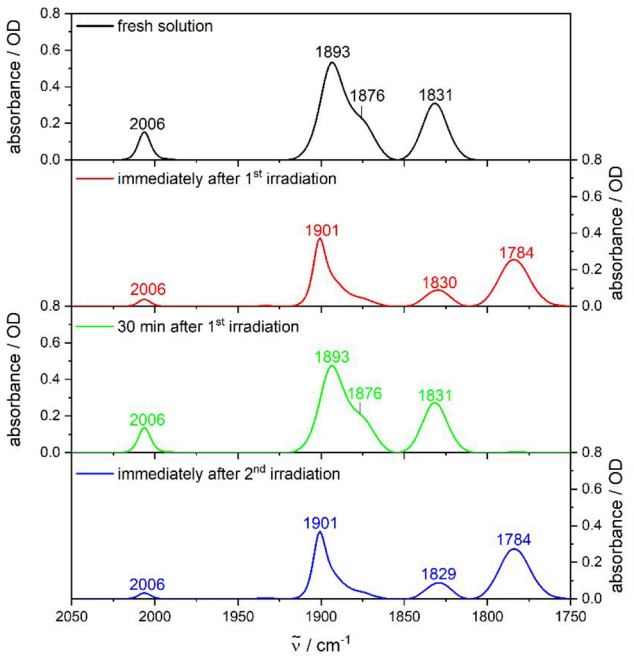

Figure 9. FTIR spectrum of a fresh solution of **2** in CH_3CN (black), immediately after the first irradiation (red), at 30 min in the dark after the first irradiation (green), and immediately after the second irradiation (blue).

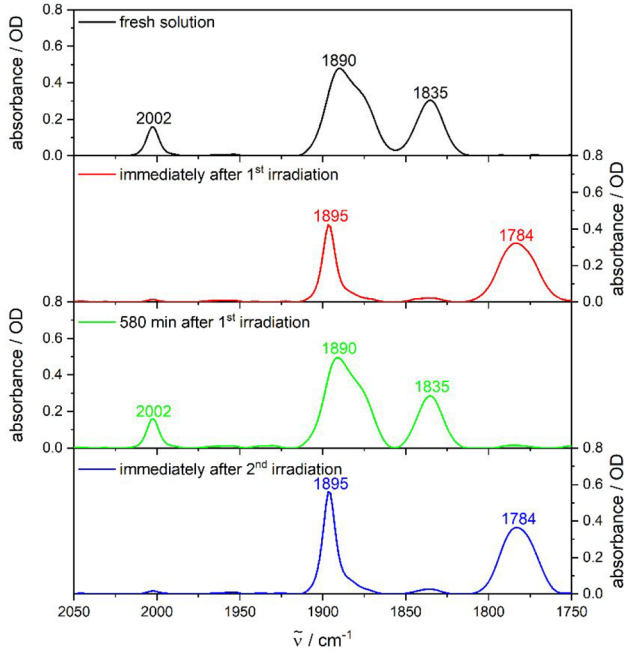

Figure 10. FTIR spectrum of a fresh solution of **2** in pyridine (black), immediately after the first irradiation (red), at 580 min in the dark after the first irradiation (green), and immediately after the second irradiation (blue).

would be protonated to the triazolium salt, which would definitely inhibit the observed reverse reaction. At the same time, dimerization, as described in the literature for the related species $[M(bpy)(CO)_3(Cl)]$ (M = Mn,[55] Re[56]), cannot be completely excluded. A large series of different potential photoproducts, including aggregates with the solvent, CO-bridged dimers, and dimers with metal−metal bonds as well as intermediate binding of free CO ligands by solvent molecules, were considered in the quantum-chemical calculations but did not lead to a good description of the measured IR spectrum.

The chromium complex **1** showed similar spectra, with the only difference being that the reactivity is lower and that one additional weak CO absorption band appears at 1928 cm^{-1} upon irradiation (Figure S48). This feature might result from the formation of a second isomer to a small extent. In addition, it should be mentioned that the dark reverse reaction is completed already after about 15 min and is thus twice as fast as that in the case of **2**, so that the metal center has an influence on the reaction dynamics. The step-scan data are analogous to the results obtained for **1** (Figures S49 and S50).

After the studies in CH_3CN, the better N-donating ligand pyridine was considered, where it should be mentioned that **1** and **2** are both stable in a pyridine solution in the dark. The full conversion of the educt species to the respective photoproduct is completed for both complexes after 5 min of irradiation (Figures 10 and S51).

The observation that almost no educt is left after this period of irradiation is explained by the better σ donation of pyridine compared to CH_3CN. Interestingly, the measured IR spectra are all analogous to the observations in CH_3CN, so that the reaction dynamics may be identical. The reverse reactions from the photoproducts back to the educts are completed after about 35 min for **1** and 10 h for **2**, so they are much slower compared to CH_3CN. This demonstrates that stable photoproducts are formed in a pyridine solution upon UV irradiation, in particular for the molybdenum(0) species.

The interesting photochemical reactivity toward pyridine incentivized us to analyze the reactivity under the presence of the bidentate ligand 2,2′-bipyridine, using CH_2Cl_2 as the solvent. For a solution of **2** saturated with 2,2′-bipyridine, a dark reaction is already observed in the first FTIR spectrum recorded immediately after preparation of the reaction mixture, which corresponds to a few tenths of seconds.

Three new weak CO bands are observed between 1925 and 2000 cm^{-1}, which do, however, not increase over time neither in the dark nor upon light excitation (Figure S52). The bleaching of the educt bands is assigned to a photochemical reaction with the solvent. Hence, the reaction with 2,2′-bipyridine is definitely incomplete with a low turnover. The observation of three CO bands might result from a loss of one CO ligand, lifting of one coordinative bond of the MIC ligand to the metal center, and coordination of the bidentate 2,2′-bipyridine ligand. However, a superimposition of additional product vibrations by the educt peaks and/or the formation of different isomers (three new peaks) cannot be excluded.

Because investigations with 2,2′-bipyridine in a CH_2Cl_2 solution gave first indications for a reaction with solvent molecules, we performed step-scan measurements for **1** and **2** in a CH_2Cl_2 solution. The obtained step-scan difference spectra are very similar to the results in CH_3CN, with the lowest-energy CO vibration being red-shifted by about 40 cm^{-1}, the energetically highest educt band showing only a bleach band without any positive peak, and the third CO motion being blue-shifted by approximately 20 cm^{-1} in the photoproduct (Figures S53−S56). This indicates that the reaction mechanism under the presence of CH_2Cl_2 may be analogous to the suggested dynamics in a CH_3CN solution with cleavage of a coordinative bond of the bidentate MIC ligand to the metal and occupation of the free coordination site

https://dx.doi.org/10.1021/acs.inorgchem.0c02537
Inorg. Chem. XXXX, XXX, XXX−XXX

by a solvent molecule. Again, the features and intensities of the difference spectrum do not change significantly over the whole step-scan experiment, so that investigations were performed on longer times scales for **2**.

An irradiation over 5 min leads to a significant decrease of the educt bands and the appearance of a new CO vibration at about 1930 cm^{-1}. Different CO bands are observed temporarily around 1925 and 1980 cm^{-1} over the next 7 h after irradiation, indicating the formation of different intermediates with a series of coordination motifs (Figure S57).

Time-Dependent [(TD-)DFT] Calculations. DFT calculations at the B3LYP/RIJCOSX/D3/def2-TZVP level of theory were carried out on **1** and **2**, as well as on their oxidized and reduced forms. The calculated bond lengths (Tables S17 and S25) from the optimized structures of both complexes are in good agreement with the experimental bond lengths obtained from single-crystal X-ray diffraction data.

The highest occupied molecular orbital (HOMO) is largely localized on the central metal atom and the two equatorial CO ligands for **1** and **2**, whereas the lowest occupied molecular orbitals (LUMOs) in both the complexes are almost exclusively localized on the chelating pyridyl-MIC ligand **L1** (Tables S12 and S21 and Figures 11 and S25).

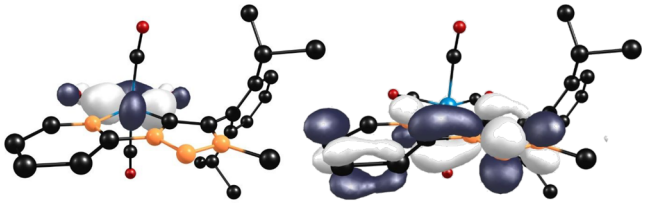

Figure 11. HOMO (left) and LUMO (right) of complex **2** (isovalue = 0.052).

Because both the first oxidation and first reduction steps of **1** are reversible on the electrochemical and spectroelectrochemical time scales, we briefly comment here on the calculated structural parameters of $\mathbf{1}^{+}$ and $\mathbf{1}^{\bullet-}$. In comparison to **1**, all of the calculated Cr−CO bond distances in $\mathbf{1}^{+}$ are strongly elongated, whereas the changes in these bond distances in $\mathbf{1}^{\bullet-}$ are only marginal (Table S17). Accordingly, the C−O bond distances in $\mathbf{1}^{+}$ are much shorter compared to those in **1**, and those in $\mathbf{1}^{\bullet-}$ display only marginal changes compared to those in **1**. The changes in the calculated bond lengths within the **L1** ligand in the three redox forms provide some further interesting trends. In **1** and $\mathbf{1}^{+}$, the changes in the bond distances within **L1** are marginal. However, when the same distances are compared between **1** and $\mathbf{1}^{\bullet-}$, some systematic changes are apparent. Within the 1,2,3-triazol-5-ylidene part of **L1**, the C1−C2 bond is shortened in $\mathbf{1}^{\bullet-}$ compared to **1**, whereas all of the other four bonds are elongated in the reduced complex in comparison to the neutral one. These observations fit nicely with the bonding/antibonding interactions between the atoms, as seen in the α-HOMO of $\mathbf{1}^{\bullet-}$ (Figure S28).

The C3−N2 bond that connects the pyridyl and MIC units in **L1** is significantly shorter in $\mathbf{1}^{\bullet-}$ than in **1**. Within the pyridyl ring, the most significant changes are in the C3−N1 and C3−C4 bond distances, both of which become longer upon moving from **1** to $\mathbf{1}^{\bullet-}$. With these optimized structures, we calculated the IR, EPR, and UV−vis−NIR spectroscopic features for the various redox forms of both complexes. In the following, we will restrict the discussion on the ground-state spectroscopic properties to the chromium complex **1** because the properties of the molybdenum complex **2** are very similar to those of **1**.

The calculated IR spectrum of **1** nicely reproduces the experimentally observed four-band pattern in the CO region (Figures 4 and 12). The calculated absolute values of the CO stretching frequencies are, however, shifted to higher energies compared to the experimentally observed ones, which can be explained by the applied harmonic approximation (Figure S13 and Table S5). Additionally, the shift of the CO bands for the reduced form of **1** in comparison to the native form is also nicely reproduced by the calculations (Figure 12 and Table S7). The calculated spectrum of $\mathbf{1}^{+}$ (Figure S16) differs significantly from the experimental spectrum. The reasons for this discrepancy are not very clear at this moment and may result from ion pairing. Further high-level quantum-chemical calculations will be required to clarify this point.

TD-DFT calculations on **1** show that the experimentally observed absorption band at 485 nm (see above) is a mixture of transitions of HOMO−2 → LUMO (23%) and HOMO−1 → LUMO (71%) (Figures S25 and S30 and Table S13). This band can thus be assigned to a mixture of d(Cr) → π^*(**L1**) MLCT and CO → **L1** ligand-to-ligand charge-transfer (LLCT) transitions. The other prominent band in the visible region at 394 nm arises from transition HOMO−2 → LUMO+1. This band can thus be assigned to predominantly d(Cr) → π^*(pyridyl) MLCT and CO → pyridyl LLCT transitions (Figure S30 and Table S13). As discussed above, upon oxidation of **1** to $\mathbf{1}^{+}$, the original bands of **1** basically decrease in intensity, with no new prominent features appearing. Thus, the bands of $\mathbf{1}^{+}$ will not be discussed further

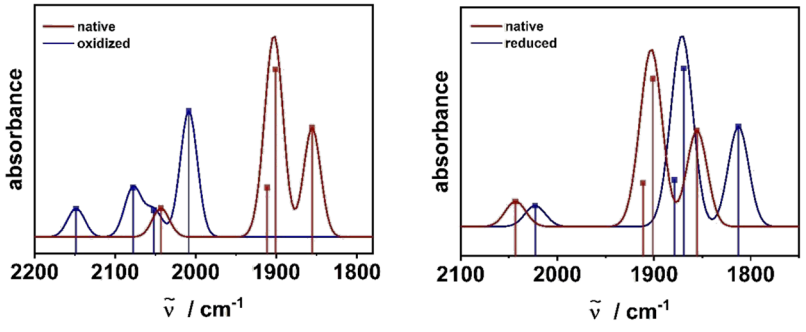

Figure 12. Calculated IR spectra of **1**, $\mathbf{1}^{+}$ (left), and $\mathbf{1}^{\bullet-}$ (right) in CH_3CN (B3LYP/RIJCOSX/D3 def2-TZVP).

https://dx.doi.org/10.1021/acs.inorgchem.0c02537
Inorg. Chem. XXXX, XXX, XXX−XXX

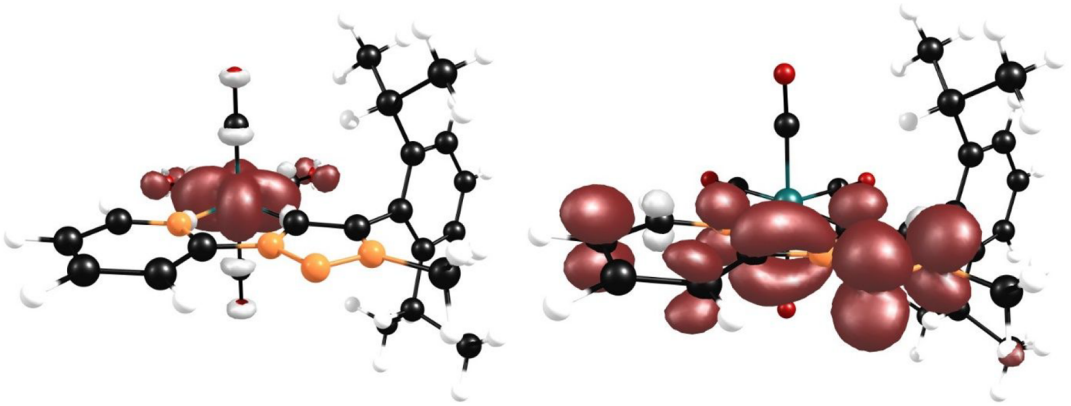

Figure 13. Spin-density plots of complex 1^+ (left) and 1^- (right) (isovalue = 0.003).

here. The reduced species $1^{\bullet-}$, on the other hand, displays multiple prominent bands in the low-energy visible and NIR regions. The origin of all of these bands is in the α-HOMO of $1^{\bullet-}$, which is delocalized over the ligand **L1** (Table S15 and Figure S28). Thus, for the reduced species, the transitions in the lower-energy visible and NIR regions can all be assigned to ligand-centered transitions. In particular, the broad NIR band centered at around 1180 nm can be assigned to a α-HOMO → α-LUMO transition, which is an intraligand-charge-transfer-type transition from the MIC to pyridyl part of **L1**. Additionally, spin-density distributions were calculated for 1^+ and $1^{\bullet-}$. In keeping with the results from EPR spectroscopy, for 1^+, the spin density is almost exclusively centered on chromium, and for $1^{\bullet-}$, the spin density is almost exclusively centered on the **L1** ligand (Figure 13 and Table S28).

CONCLUSIONS

In summary, we have presented here the synthesis and characterization of the first examples of chromium(0) and molydenum(0) complexes with a MIC-containing ligand of the 1,2,3-triazol-5-ylidene type (together with an additional pyridyl donor).

A combination of IR, EPR, and UV−vis−NIR spectroelectrochemical measurements shows that the oxidation step is metal-centered and completely reversible for the chromium(0) complex.[45,46] This result is a confirmation that the MIC ligands can support reversible redox processes at metal centers by compensating for the electron loss through their strong donating power. The first reduction step for both complexes is reversible for both complexes and almost exclusively centered on the pyridyl-MIC ligand. This is also the first report on a thorough characterization of a transition-metal-bound MIC radical. DFT and TD-DFT calculations were performed to further understand and support the aforementioned spectroscopic data.

The photochemical reactivity under the presence of different organic ligands was investigated by time-resolved (step-scan) FTIR spectroscopy, with the formation of metastable photoproducts reacting back to the educt species in slow reverse reactions. The reaction mechanism will be further elucidated by high-level quantum-chemical calculations, but the presented results already show that the irreversible loss of a CO ligand and occupation of a free coordination site by a solvent molecule, which are typically observed for homoleptic $M(CO)_6$ and heteroleptic $M(CO)_4L_2$ transition-metal complexes, are definitely not observed for the MIC-containing systems presented in this work because of the unexpected reversibility.

ASSOCIATED CONTENT

Supporting Information

The Supporting Information is available free of charge at https://pubs.acs.org/doi/10.1021/acs.inorgchem.0c02537.

Experimental section, NMR spectra, electrochemistry measurements, photophysical measurements, crystallographic details and molecular structures, and DFT (PDF)

Accession Codes

CCDC 2023753 and 2023754 contain the supplementary crystallographic data for this paper. These data can be obtained free of charge via www.ccdc.cam.ac.uk/data_request/cif, or by emailing data_request@ccdc.cam.ac.uk, or by contacting The Cambridge Crystallographic Data Centre, 12 Union Road, Cambridge CB2 1EZ, UK; fax: +44 1223 336033.

AUTHOR INFORMATION

Corresponding Authors

Markus Gerhards − *Department of Chemistry and Research Center Optimas, Technische Universität Kaiserslautern, 67663 Kaiserslautern, Germany;* orcid.org/0000-0002-8748-2940; Email: gerhards@chemie.uni-kl.de

Biprajit Sarkar − *Lehrstuhl für Anorganische Koordinationschemie, Universität Stuttgart, D-70569 Stuttgart, Germany; Institut für Chemie und Biochemie, Freie Universität Berlin, 14195 Berlin, Germany;* orcid.org/0000-0003-4887-7277; Email: biprajit.sarkar@iac.uni-stuttgart.de

Authors

Tobias Bens − *Lehrstuhl für Anorganische Koordinationschemie, Universität Stuttgart, D-70569 Stuttgart, Germany; Institut für Chemie und Biochemie, Freie Universität Berlin, 14195 Berlin, Germany*

Pit Boden − *Department of Chemistry and Research Center Optimas, Technische Universität Kaiserslautern, 67663 Kaiserslautern, Germany*

Patrick Di Martino-Fumo − *Department of Chemistry and Research Center Optimas, Technische Universität Kaiserslautern, 67663 Kaiserslautern, Germany*

Julia Beerhues − *Lehrstuhl für Anorganische Koordinationschemie, Universität Stuttgart, D-70569 Stuttgart, Germany; Institut für Chemie und Biochemie, Freie Universität Berlin, 14195 Berlin, Germany*

https://dx.doi.org/10.1021/acs.inorgchem.0c02537
Inorg. Chem. XXXX, XXX, XXX−XXX

Uta Albold − *Institut für Chemie und Biochemie, Freie Universität Berlin, 14195 Berlin, Germany*
Sebastian Sobottka − *Institut für Chemie und Biochemie, Freie Universität Berlin, 14195 Berlin, Germany*
Nicolás I. Neuman − *Institut für Chemie und Biochemie, Freie Universität Berlin, 14195 Berlin, Germany; Instituto de Desarrollo Tecnológico para la Industria Química, INTEC, UNL-CONICET, 3000 Santa Fe, Argentina;* orcid.org/0000-0003-3368-0228

Complete contact information is available at: https://pubs.acs.org/10.1021/acs.inorgchem.0c02537

Notes

The authors declare no competing financial interest.

■ ACKNOWLEDGMENTS

The high-performance computing facilities at ZEDAT of Freie Universität Berlin are acknowledged for access to computing resources. The core facility (BioSupraMol) is gratefully acknowledged. The authors are grateful to the DFG Priority Program SPP 2102 "Light-controlled reactivity of metal complexes" (SA 1840/7-1 and GE 961/10-1) for financial support. N.I.N. is grateful to the Alexander von Humboldt Foundation for a postdoctoral fellowship.

■ DEDICATION

Dedicated to Prof. Christoph Janiak on the occasion of his 60th birthday.

■ REFERENCES

(1) Guisado-Barrios, G.; Bouffard, J.; Donnadieu, B.; Bertrand, G. Crystalline 1H-1,2,3-Triazol-5-ylidenes: New Stable Mesoionic Carbenes (MICs). *Angew. Chem., Int. Ed.* **2010**, *49*, 4759−4762.
(2) Mathew, P.; Neels, A.; Albrecht, M. 1,2,3-Triazolylidenes as Versatile Abnormal Carbene Ligands for Late Transition Metals. *J. Am. Chem. Soc.* **2008**, *130*, 13534−13535.
(3) Crowley, J. D.; Lee, A.-L.; Kilpin, K. J. 1,3,4-Trisubtituted-1,2,3-Triazol-5-ylidene 'Click' Carbene Ligands: Synthesis, Catalysis and Self-Assembly. *Aust. J. Chem.* **2011**, *64*, 1118−1132.
(4) Guisado-Barrios, G.; Soleilhavoup, M.; Bertrand, G. 1 H-1,2,3-Triazol-5-ylidenes: Readily Available Mesoionic Carbenes. *Acc. Chem. Res.* **2018**, *51*, 3236−3244.
(5) Schweinfurth, D.; Hettmanczyk, L.; Suntrup, L.; Sarkar, B. Metal Complexes of Click-Derived Triazoles and Mesoionic Carbenes: Electron Transfer, Photochemistry, Magnetic Bistability, and Catalysis. *Z. Anorg. Allg. Chem.* **2017**, *643*, 554−584.
(6) Vivancos, Á.; Segarra, C.; Albrecht, M. Mesoionic and Related Less Heteroatom-Stabilized N-Heterocyclic Carbene Complexes: Synthesis, Catalysis, and Other Applications. *Chem. Rev.* **2018**, *118*, 9493−9586.
(7) Corbucci, I.; Petronilho, A.; Müller-Bunz, H.; Rocchigiani, L.; Albrecht, M.; Macchioni, A. Substantial Improvement of Pyridine-Carbene Iridium Water Oxidation Catalysts by a Simple Methyl-to-Octyl Substitution. *ACS Catal.* **2015**, *5*, 2714−2718.
(8) Kleinhans, G.; Guisado-Barrios, G.; Liles, D. C.; Bertrand, G.; Bezuidenhout, D. I. A rhodium(I)-oxygen adduct as a selective catalyst for one-pot sequential alkyne dimerization-hydrothiolation tandem reactions. *Chem. Commun.* **2016**, *52*, 3504−3507.
(9) Suntrup, L.; Stein, F.; Klein, J.; Wilting, A.; Parlane, F. G. L.; Brown, C. M.; Fiedler, J.; Berlinguette, C. P.; Siewert, I.; Sarkar, B. Rhenium Complexes of Pyridyl-Mesoionic Carbenes: Photochemical Properties and Electrocatalytic CO_2 Reduction. *Inorg. Chem.* **2020**, *59*, 4215−4227.
(10) van der Meer, M.; Glais, E.; Siewert, I.; Sarkar, B. Electrocatalytic Dihydrogen Production with a Robust Mesoionic Pyridylcarbene Cobalt Catalyst. *Angew. Chem., Int. Ed.* **2015**, *54*, 13792−13795.
(11) Woods, J. A.; Lalrempuia, R.; Petronilho, A.; McDaniel, N. D.; Müller-Bunz, H.; Albrecht, M.; Bernhard, S. Carbene iridium complexes for efficient water oxidation: scope and mechanistic insights. *Energy Environ. Sci.* **2014**, *7*, 2316−2328.
(12) Maity, R.; van der Meer, M.; Sarkar, B. Redox-active multinuclear Pd(II) complexes with bis- and tris-mesoionic carbenes. *Dalton Trans.* **2015**, *44*, 46−49.
(13) Suntrup, L.; Klenk, S.; Klein, J.; Sobottka, S.; Sarkar, B. Gauging Donor/Acceptor Properties and Redox Stability of Chelating Click-Derived Triazoles and Triazolylidenes: A Case Study with Rhenium-(I) Complexes. *Inorg. Chem.* **2017**, *56*, 5771−5783.
(14) Baschieri, A.; Monti, F.; Matteucci, E.; Mazzanti, A.; Barbieri, A.; Armaroli, N.; Sambri, L. A Mesoionic Carbene as Neutral Ligand for Phosphorescent Cationic Ir(III) Complexes. *Inorg. Chem.* **2016**, *55*, 7912−7919.
(15) Brown, D. G.; Sanguantrakun, N.; Schulze, B.; Schubert, U. S.; Berlinguette, C. P. Bis(tridentate) Ruthenium-Terpyridine Complexes Featuring Microsecond Excited-State Lifetimes. *J. Am. Chem. Soc.* **2012**, *134*, 12354−12357.
(16) Chábera, P.; Liu, Y.; Prakash, O.; Thyrhaug, E.; Nahhas, A. E.; Honarfar, A.; Essén, S.; Fredin, L. A.; Harlang, T. C. B.; Kjær, K. S.; et al. A low-spin Fe(iii) complex with 100-ps ligand-to-metal charge transfer photoluminescence. *Nature* **2017**, *543*, 695−699.
(17) Hettmanczyk, L.; Spall, S. J. P.; Klenk, S.; van der Meer, M.; Hohloch, S.; Weinstein, J. A.; Sarkar, B. Structural, Electrochemical, and Photochemical Properties of Mono- and Digold(I) Complexes Containing Mesoionic Carbenes. *Eur. J. Inorg. Chem.* **2017**, *2017*, 2112−2121.
(18) Kleinhans, G.; Chan, A. K.-W.; Leung, M.-Y.; Liles, D. C.; Fernandes, M. A.; Yam, V. W.-W.; Fernández, I.; Bezuidenhout, D. I. Synthesis and Photophysical Properties of T-Shaped Coinage-Metal Complexes. *Chem. - Eur. J.* **2020**, *26*, 6993−6998.
(19) Leigh, V.; Ghattas, W.; Lalrempuia, R.; Müller-Bunz, H.; Pryce, M. T.; Albrecht, M. Synthesis, Photo-, and Electrochemistry of Ruthenium Bis(bipyridine) Complexes Comprising a N-heterocyclic Carbene Ligand. *Inorg. Chem.* **2013**, *52*, 5395−5402.
(20) Matteucci, E.; Monti, F.; Mazzoni, R.; Baschieri, A.; Bizzarri, C.; Sambri, L. Click-Derived Triazolylidenes as Chelating Ligands: Achievement of a Neutral and Luminescent Iridium(III)-Triazolide Complex. *Inorg. Chem.* **2018**, *57*, 11673−11686.
(21) Sarkar, B.; Suntrup, L. Illuminating Iron: Mesoionic Carbenes as Privileged Ligands in Photochemistry. *Angew. Chem., Int. Ed.* **2017**, *56*, 8938−8940.
(22) Soellner, J.; Tenne, M.; Wagenblast, G.; Strassner, T. Phosphorescent Platinum(II) Complexes with Mesoionic 1H-1,2,3-Triazolylidene Ligands. *Chem. - Eur. J.* **2016**, *22*, 9914−9918.
(23) Suntrup, L.; Stein, F.; Hermann, G.; Kleoff, M.; Kuss-Petermann, M.; Klein, J.; Wenger, O. S.; Tremblay, J. C.; Sarkar, B. Influence of Mesoionic Carbenes on Electro- and Photoactive Ru and Os Complexes: A Combined (Spectro-)Electrochemical, Photochemical, and Computational Study. *Inorg. Chem.* **2018**, *57*, 13973−13984.
(24) Hettmanczyk, L.; Manck, S.; Hoyer, C.; Hohloch, S.; Sarkar, B. Heterobimetallic complexes with redox-active mesoionic carbenes as metalloligands: electrochemical properties, electronic structures and catalysis. *Chem. Commun.* **2015**, *51*, 10949−10952.
(25) Hettmanczyk, L.; Suntrup, L.; Klenk, S.; Hoyer, C.; Sarkar, B. Heteromultimetallic Complexes with Redox-Active Mesoionic Carbenes: Control of Donor Properties and Redox-Induced Catalysis. *Chem. - Eur. J.* **2017**, *23*, 576−585.
(26) Klenk, S.; Rupf, S.; Suntrup, L.; van der Meer, M.; Sarkar, B. The Power of Ferrocene, Mesoionic Carbenes, and Gold: Redox-Switchable Catalysis. *Organometallics* **2017**, *36*, 2026−2035.
(27) Vanicek, S.; Beerhues, J.; Bens, T.; Levchenko, V.; Wurst, K.; Bildstein, B.; Tilset, M.; Sarkar, B. Oxidative Access via Aqua Regia to an Electrophilic, Mesoionic Dicobaltoceniumyltriazolylidene Gold-(III) Catalyst. *Organometallics* **2019**, *38*, 4383−4386.

(28) Vanicek, S.; Podewitz, M.; Stubbe, J.; Schulze, D.; Kopacka, H.; Wurst, K.; Müller, T.; Lippmann, P.; Haslinger, S.; Schottenberger, H.; et al. Highly Electrophilic, Catalytically Active and Redox-Responsive Cobaltoceniumyl and Ferrocenyl Triazolylidene Coinage Metal Complexes. *Chem. - Eur. J.* **2018**, *24*, 3742−3753.
(29) Baltrun, M.; Watt, F. A.; Schoch, R.; Wölper, C.; Neuba, A. G.; Hohloch, S. A new bis-phenolate mesoionic carbene ligand for early transition metal chemistry. *Dalton Trans.* **2019**, *48*, 14611−14625.
(30) Vichova, J.; Hartl, F.; Vlček, A., Jr. Wavelength-Dependent Photosubstitution and Excited-State Dynamics of $[Cr(CO)_4(2,2'$-bipyridine)]: A Quantum Yield and Picosecond Absorption Atudy. *J. Am. Chem. Soc.* **1992**, *114*, 10903−10910.
(31) Stufkens, D. J. Spectroscopy, Photophysics and Photochemistry of Zerovalent Transition Metal α-Diimine Complexes. *Coord. Chem. Rev.* **1990**, *104*, 39−112.
(32) Vlček, A., Jr. Highlights of spectroscopy, photochemistry and electrochemistry of $[M(CO)_4(\alpha$-diimine)] complexes, M = Cr, Mo, W. *Coord. Chem. Rev.* **2002**, *230*, 225−242.
(33) Tory, J.; Setterfield-Price, B.; Dryfe, R. A. W.; Hartl, F. $[M(CO)_4$ (2,2′-bipyridine)] (M = Cr, Mo, W) Complexes as Efficient Catalysts for Electrochemical Reduction of CO_2 at a Gold Electrode. *ChemElectroChem* **2015**, *2*, 213−217.
(34) Schoonover, J. R.; Strouse, G. F.; Omberg, K. M.; Dyer, R. B. Time-Resolved, Step-Scan FTIR Spectroscopy of Excited States of Transition Metal Complexes. *Comments Inorg. Chem.* **1996**, *18*, 165−188.
(35) Skopintsev, P.; Ehrenberg, D.; Weinert, T.; James, D.; Kar, R. K.; Johnson, P. J. M.; Ozerov, D.; Furrer, A.; Martiel, I.; Dworkowski, F.; et al. Femtosecond-to-millisecond structural changes in a light-driven sodium pump. *Nature* **2020**, *583*, 314−318.
(36) Smith, G. D.; Hutson, M. S.; Lu, Y.; Tierney, M. T.; Grinstaff, M. W.; Palmer, R. A. Step-Scan FT-IR Time-Resolved Spectroscopy in the Solid State. *Appl. Spectrosc.* **2001**, *55*, 637−641.
(37) Treiling, S.; Wang, C.; Förster, C.; Reichenauer, F.; Kalmbach, J.; Boden, P.; Harris, J. P.; Carrella, L. M.; Rentschler, E.; Resch-Genger, U.; et al. Luminescence and Light-Driven Energy and Electron Transfer from an Exceptionally Long-Lived Excited State of a Non-Innocent Chromium(III) Complex. *Angew. Chem., Int. Ed.* **2019**, *58*, 18075−18085.
(38) Wagner, H. E.; Di Martino-Fumo, P.; Boden, P.; Zimmer, M.; Klopper, W.; Breher, F.; Gerhards, M. Structural Characterization and Lifetimes of Triple-Stranded Helical Coinage Metal Complexes: Synthesis, Spectroscopy and Quantum Chemical Calculations. *Chem. - Eur. J.* **2020**, *26*, 10743−10751.
(39) Zimmer, M.; Rupp, F.; Singer, P.; Walz, F.; Breher, F.; Klopper, W.; Diller, R.; Gerhards, M. Time-resolved IR spectroscopy of a trinuclear palladium complex in solution. *Phys. Chem. Chem. Phys.* **2015**, *17*, 14138−14144.
(40) Harris, A.; Saita, M.; Resler, T.; Hughes-Visentin, A.; Maia, R.; Pranga-Sellnau, F.; Bondar, A.-N.; Heberle, J.; Brown, L. S. Molecular details of the unique mechanism of chloride transport by a cyanobacterial rhodopsin. *Phys. Chem. Chem. Phys.* **2018**, *20*, 3184−3199.
(41) Schroeder, L.; Oldemeyer, S.; Kottke, T. Time-Resolved Infrared Spectroscopy on Plant Cryptochrome-Relevance of Proton Transfer and ATP Binding for Signaling. *J. Phys. Chem. A* **2018**, *122*, 140−147.
(42) Schultz, H. R.; Krav-Ami, S. When the ligands go marching in: a step-scan Fourier transform infrared spectroscopic study of ligand attack at the transient species $W(CO)_5$(CyH). *J. Chem. Soc., Dalton Trans.* **1999**, 115−117.
(43) Moore, B. D.; Poliakoff, M.; Simpson, M. B.; Turner, J. J. Fast Time-Resolved FTIR Detection of Short-Lived Photochemical Transient Species in Solution: A Direct Comparison with IR Laser Spectroscopy. *J. Phys. Chem.* **1985**, *89*, 850−853.
(44) Torres-Alacan, J.; Vöhringer, P. Photolysis of a High-Spin Azidoiron(III) Complex Studied by Time-Resolved Fourier-Transform Infrared Spectroscopy. *Chem. - Eur. J.* **2017**, *23*, 6746−6751.
(45) Bohnenberger, J.; Feuerstein, W.; Himmel, D.; Daub, M.; Breher, F.; Krossing, I. Stable salts of the hexacarbonyl chromium(I) cation and its pentacarbonyl-nitrosyl chromium(I) analogue. *Nat. Commun.* **2019**, *10*, 624.
(46) Bohnenberger, J.; Schmitt, M.; Feuerstein, W.; Krummenacher, I.; Butschke, B.; Czajka, J.; Malinowski, P. J.; Breher, F.; Krossing, I. Completing the triad: synthesis and full characterization of homoleptic and heteroleptic carbonyl and nitrosyl complexes of the group VI metals. *Chem. Sci.* **2020**, *11*, 3592−3603.
(47) Vlček, A., Jr.; Baumann, F.; Kaim, W.; Grevels, F.-W.; Hartl, F. Electron distribution in the $Cr(CO4(bpy)^{\bullet-}$ (bpy = 2,2′-bipyridine) radical anion as reveal by EPR spectroscopy and IR spectroelectrochemistry of ^{13}C-enriched species. *J. Chem. Soc., Dalton Trans.* **1998**, 215−220.
(48) Kaim, W. Concepts for metal complex chromophores absorbing in the near infrared. *Coord. Chem. Rev.* **2011**, *255*, 2503−2513.
(49) Schultz, H. R.; Krav-Ami, S. When the ligand go marching in: a step-scan Fourier transform infrared spectroscopic study of ligand attack at the transient species $W(CO)_5$(CyH). *J. Chem. Soc., Dalton Trans.* **1999**, 115−117.
(50) Schaffner, K.; Grevels, F.-W. Infrared Spectroscopy of Excited States and Transient in Photochemistry. *J. Mol. Struct.* **1988**, *173*, 51−65.
(51) Greetham, G. M.; Sole, D.; Clark, I. P.; Parker, A. W.; Pollard, M. R.; Towrie, M. Time-resolved multiple probe spectroscopy. *Rev. Sci. Instrum.* **2012**, *83*, 103107.
(52) Manuta, D. M.; Lees, A. J. Emission and Photochemistry of $M(CO)_4$(diimine) (M = Cr, Mo, W) Complexes in Room-Temperature Solution. *Inorg. Chem.* **1986**, *25*, 1354−1359.
(53) Moore, K. J.; Petersen, J. D. Synthesis, Characterization and Photochemistry of some Monometallic and Bimetallic 2,2′-Bipyrimidine Complexes of Chromum and Tungsten Carbonyls. *Polyhedron* **1983**, *2*, 279−284.
(54) Kianfar, E.; Kaiser, M.; Knör, G. Synthesis, characterization and photoreactivity of rhenium and molybdenum carbonyl complexes with iminopyridine ligands. *J. Organomet. Chem.* **2015**, *799−800*, 13−18.
(55) Hartl, F.; Rossenaar, B. D.; Stor, G. J.; Stufkens, D. J. Role of an electrontransfer chain reaction in the unusual photochemical formation of fivecoordinated anions $[Mn(CO)_3$(diimine)]$^-$ from fac[Mn(X)$(CO)_3$(diimine)] (X = halide) at low temperatures. *Red. Trav. Chim. Pays-Bas* **1995**, *114*, 565−570.
(56) Lang, P.; Giereth, R.; Tschierlei, S.; Schwalbe, M. Unexpected wavelength dependency of the photocatalytic CO_2 reduction performance of the well-known (bpy)Re$(CO)_3$Cl complex. *Chem. Commun.* **2019**, *55*, 600−603.

https://dx.doi.org/10.1021/acs.inorgchem.0c02537
Inorg. Chem. XXXX, XXX, XXX−XXX